ASCE

Development of Time–Depth–Damage Functions for Flooded Flexible Pavements

Narges Matini[1]; Yaning Qiao[2]; and Jo E. Sias, M.ASCE[3]

Abstract: The first step toward building pavement structures that are resilient to flooding is to have a proper understanding of the impact of inundation on the pavement. Depth-damage functions have been developed and are widely used to quantify flood-induced damage to buildings. However, such damage functions do not exist for roadway pavements. The objective of this study is to develop a methodological framework to model postflooding road damage by identifying the importance of several parameters including flood duration, flood depth, flood pattern (including real flood data), transfer functions, pavement materials, and analysis location. Pavement serviceability and costs are introduced into the evaluation as well. The long-term goal is a tool for decision makers to use in planning and management of flooding events for more resilient pavements and allocation of budgets. It is established that the most important parameters that should be accounted for by decision makers are the flood duration, combination of the materials, critical location on the roadway (both vertical and lateral), and use of appropriate transfer functions. Opening the roadway to traffic immediately after the floodwater recedes will lead to earlier and more significant deterioration of the pavement and more costly maintenance and reconstruction. **DOI: 10.1061/JPEODX.0000352.**

Author keywords: Resilience; Flexible pavements; Flooding.

Introduction

The recent increase in the frequency and magnitude of infrastructure impacts from extreme events has raised awareness of the urgent need to improve the resilience of vital infrastructure and assets such as pavements. The knowledge base with respect to pavement resilience is rapidly expanding but still relatively immature. Flooding associated with extreme events, sea-level rise, and nuisance flooding related to tides are primary concerns for pavement infrastructure. The focus of most of the previous studies has largely been on the return of mobility (termed here as functional resilience). There is a lack of sufficient technical details and analysis to guide agencies on dealing with the return of, or management of losses in, structural integrity (termed here as structural resilience). The priority of agencies and the demand of the public is to restore the functionality of the services for economic and social reasons. However, this demand does not mean that structural aspects can be ignored. Structural disruptions manifest over a much longer timescale and so their cumulative effect on services may exceed that of the initial disruption in the long run. Functional disruptions only reflect on the short-term effect of the event on the pavement, and management decisions just for the purpose of restoring the functionality after the events may lead to temporary remedies. However, structural disruptions manifest largely due to decisions made at the design stage, which occurs years or even decades before the event. In order to approach this problem, it is imperative to look closely at the structural impact of flooding on flexible pavements. To understand the impact of flooding on pavement structures, the influential elements and their potential effects need to be evaluated. These elements can range from structural elements such as pavement thickness or a combination of the pavement materials and their properties to characteristics of a flooding event, including flood depth and duration. This then needs to be translated to practical tangible parameters, the type of tool that an agency needs. Fundamentally, the structural impact of flooding on pavements is important to agencies so that they use this knowledge to evaluate and minimize the cost of rehabilitation and reconstruction of flooded pavements.

The structural evaluation of the effect of flooding on pavements mostly relies on the pavement condition surveys occasionally coupled with performance models after events. Elshaer and Daniel (2018) reviewed previous case studies to understand the magnitude of the impact of flooding but not necessarily all the variables or factors that might impact the process. The previous case studies were completed to evaluate the impacts of Hurricane Katrina (Chen and Zhang 2014; Gaspard et al. 2007; Zhang et al. 2008), the Missouri River flooding of 2011 (Vennapusa et al. 2013), and flooding in 2011 in Queensland, Australia, (Sultana et al. 2016) on flooded pavement deterioration. The collective results indicated that flooding could cause an 18 to 30 percent reduction in the structural performance of pavements. They also studied the structural response and changes in the capacity of inundated pavements using layered elastic analysis (LEA) to compare the resultant stresses and strains due to changes in soil modulus and empirical approaches to evaluate changes in the American Association of State Highway and Transportation Officials (AASHTO) design structural number (SN). The results show increases by up to 80% in vertical strains, 15% in horizontal strains, and 40% in the required SN to withstand the same level of traffic. In a recent study, an accelerated pavement test (APT) coupled with a nonlinear elastic (NLE) modeling approach was used to investigate the development of permanent

[1]Graduate Research Assistant, Dept. of Civil, Construction, and Environmental Engineering, North Carolina State Univ., 915 Partners Way, Raleigh, NC 27695. ORCID: https://orcid.org/0000-0003-2636-311X. Email: nmatini@ncsu.edu

[2]Associate Professor, School of Mechanics and Civil Engineering, China Univ. of Mining and Technology, Xuzhou, Jiangsu Province 22116, China (corresponding author). ORCID: https://orcid.org/0000-0002-9051-8406. Email: yaning.qiao@cumt.edu.cn; qyn35@hotmail.com

[3]Professor, Dept. of Civil and Environmental Engineering, Univ. of New Hampshire, Kingsbury Hall, Durham, NH 03824. ORCID: https://orcid.org/0000-0001-5284-0392. Email: Jo.Sias@unh.edu

Note. This manuscript was submitted on January 19, 2021; approved on December 14, 2021; published online on February 22, 2022. Discussion period open until July 22, 2022; separate discussions must be submitted for individual papers. This paper is part of the ***Journal of Transportation Engineering, Part B: Pavements***, © ASCE, ISSN 2573-5438.

deformation under different moisture conditions which were altered by raising the groundwater table (GWT) (Fladvad and Erlingsson, forthcoming). Increased GWT accelerates the accumulation of permanent deformations in structures with open-graded and well-graded subbase materials.

Months after Hurricane Katrina and Hurricane Rita, pavement testing procedures including falling weight deflectometer (FWD), ground-penetrating radar, and dynamic cone penetrometer (DCP) testing along with coring were conducted on eight roadways in New Orleans (Gaspard et al. 2007). The FWD testing provided pavement SN along with subgrade modulus; the DCP provided verification of the base and subgrade moduli; the coring provided thicknesses and verification of moisture damage. For one of the roadways, data from before the hurricane was available and for the other seven roadways, flood mapping was used to identify nonsubmerged and submerged locations. Testing data from nonsubmerged and submerged locations were considered as a control set and an experimental set, respectively. Three structural parameters including the first sensor deflection (D_1), effective structural number (SN_{eff}), and subgrade resilient modulus were statistically compared, and the structural loss was determined. As part of the Federal Highway Administration (FHWA) pilot study for asset management related to extreme events, the impact of Hurricane Harvey on different pavement structures in the Houston District was evaluated (Texas DOT 2019). The flooded pavements were simulated by the Texas Mechanistic-Empirical (TxME), and the long-term impact of flooding on damage and the service life of inundated flexible pavements were determined.

Important limitations with the evaluation of flooded pavements based on the on-site experiments are: (1) the tests had to be conducted several months after the waters receded and possible additional damage from debris haul trucks that continued to travel over these weakened structures cannot be determined, and (2) data from before the event is mostly unavailable and using data from similar nonsubmerged locations as control set adds to the uncertainty of the final results.

An extensive study was conducted focusing on evaluating flooded pavements and finding the appropriate time after a flooding event to open roads to traffic (Daniel et al. 2018). This is important since immediately after the floodwater recedes, the pavement is still weak due to fully or partly saturated unbound layers, and opening it to traffic can cause long-term and fundamental damage to the pavement and leads to extra rehabilitation costs. A comprehensive research study was conducted to determine the impact by modeling the postflooding hydrology and hydraulic conditions, laboratory testing for moisture damage of pavement materials, modeling inundated pavement structures, and optimization of operational decision making based on the expected subsequent cost of operation decisions, risk of road damage, preferences and judgment, data and results from visual inspections, and nondestructive test results.

Few studies focus on the cost analysis of flooded pavements, and one of the reasons for that is the cost analysis varies by agency because each has its own policies and priorities for extreme events. Another reason is several elements have direct and indirect effects on costs that should be considered for a flooded pavement system, and a comprehensive study is needed to monetize the structural damage to the flooded pavement. In the study that was conducted to determine the effect of Hurricane Katrina and Rita on roadways in New Orleans, the loss of SN was converted to the loss of pavement thickness that was translated into cost using the unit cost associated with rehabilitation (Gaspard et al. 2007). In another study, a methodology was developed to estimate the increase in damage and rehabilitation costs due to the impact of Hurricane Harvey on pavement structures in southeast Texas and southwest Louisiana (Romanoschi 2019). The damage caused by flooding was determined directly based on the increase in moisture in foundation layers or indirectly as a result of the increase in heavy traffic during debris removal. Also, the increase in cost was determined in terms of earlier than anticipated rehabilitation needs and the increase in fuel consumption caused by the increase in pavement roughness.

The building and insurance industries have developed depth-damage functions that are widely used to quantify flood-induced damage for buildings (Scawthorn et al. 2006; Pistrika and Jonkman 2010; Pistrika et al. 2014). Inspired by this, a framework for determining depth-damage functions for flexible pavement structures was developed to overcome the limitations associated with current approaches for determining flood-induced pavement damage and costs. The focus was on impacts due to inundation and did not consider damage due to flowing water (e.g., washouts). These functions were developed based on a synthetic approach that considers damage processes and mechanisms. The synthetic approach is appropriate for cases where limited flood data are available and has been used previously for evaluating the damage to buildings using stochastic methods and analytical representation of failure mechanism of building components (Nadal et al. 2010). The inundation impacts are primarily caused by the loss of layer stiffness due to moisture weakening of the granular layers and cumulative damage under repeated traffic loads (Zhang et al. 2008). When pavements are under flooding conditions, unbound and subgrade materials are weakened by infiltrating floodwater and it takes time for pavements to become saturated and to subsequently recover once floodwaters have receded (Dawson 2009; Salour and Erlingsson 2013). During periods of saturation and recovery, pavements lose stiffness due to excessive moisture and the pavement traffic bearing capacity can be significantly reduced (Zhang et al. 2008; Gaspard et al. 2007; Vennapusa et al. 2013). The rate at which damage accumulates in a pavement can accelerate compared to nonflood conditions under the same level of traffic, typically in the form of rutting and cracking (Khan et al. 2017; Mallick et al. 2017; Sultana et al. 2016). The inundation impacts occur anywhere pavements are flooded and are not visible until significant damage appears on the pavement surface.

Objective

The objective of this study is to develop a methodological framework for establishing time–depth–damage functions using the synthetic approach. The main contribution of this study is that it enables the quantification of flood-induced damage on pavements, which is a current gap in the field. Various factors that can impact flooding induced pavement damage are considered in this study; specifically, this work is designed to identify the importance of parameters including flood duration, flood depth, flood pattern (including real flood data), the transfer function for damage calculation, pavement material, and analysis location. In addition, pavement serviceability and costs are evaluated. The long-term goal is a tool for decision makers to use in planning and the management of flooding events for more resilient flexible pavements and allocation of budgets.

Methodology

Flooding is defined in this study as whenever the water level overtops the pavement surface; this may be due to either precipitation, riverine flooding, or coastal flooding. The following tasks are set to achieve the research goal, including: (1) model the changes in the moisture field of flooded pavements using the finite element

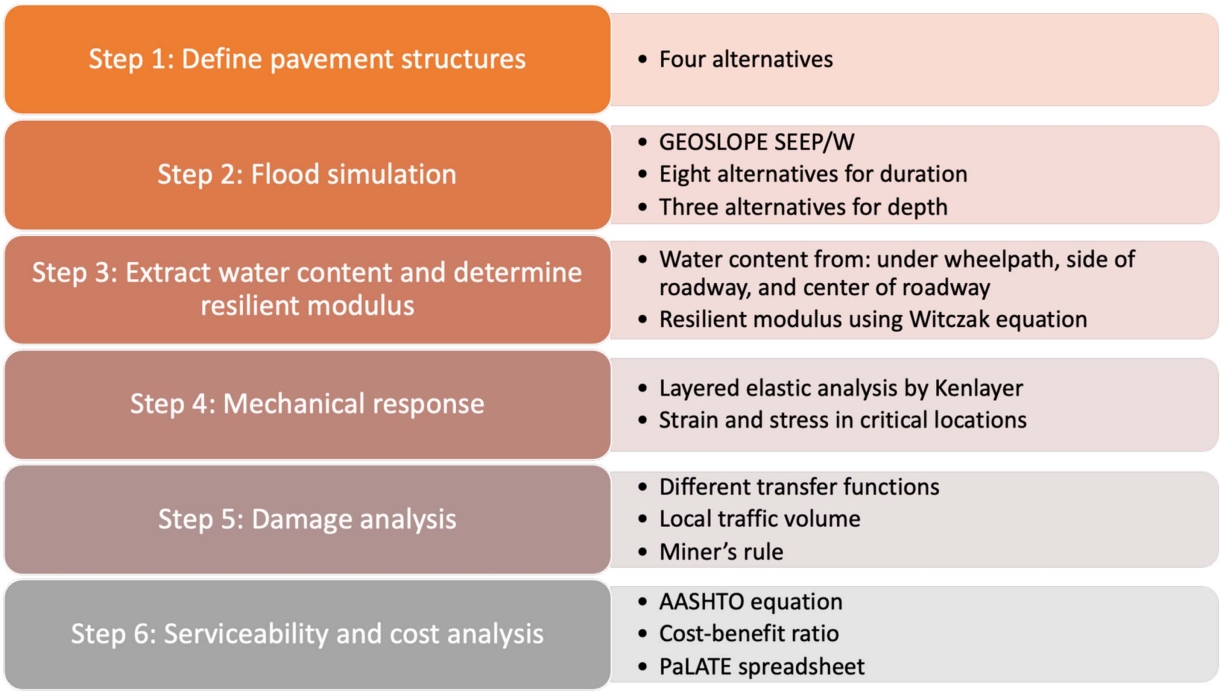

Fig. 1. The overall approach.

Table 1. Pavement structures properties

Structure type	Structure code	Base layer material	Subgrade material	Asphalt concrete layer thickness (cm)	Base layer thickness (cm)
Structure 1	OGS	Open-graded gravel	Sand	15	33
Structure 2	OGC	Open-graded gravel	Clay	15	33
Structure 3	DGS	Dense-graded gravel	Sand	15	33
Structure 4	DGC	Dense-graded gravel	Clay	15	33

method (FEM); (2) estimate moisture effects on pavement stiffness; (3) derive damage due to flooding and develop time–depth–damage functions; and (4) determine the impact on serviceability deterioration and maintenance/reconstruction costs. To achieve these tasks, the FEM, LEA, and AASHTO equation were used to simulate the performance of flooded pavements at different time intervals (before, during, and after the flood). The overall approach will be discussed in detail in the following sections, and it is summarized in Fig. 1.

The steps of the overall approach are as follows:

Step 1: Define Pavement Structures

In this study, one combination of layer thicknesses was selected to evaluate merely the impact of changing materials. In addition to open-graded gravel, dense-graded gravel was considered as the base material. Clay and sand were evaluated as subgrade materials in this study. It was assumed that the moduli values for asphalt concrete, gravel base, sand subgrade, and clay subgrade are 500, 38, 10, and 4 ksi, respectively. Four pavement structures, shown in Table 1, were analyzed to determine the performance of these combinations of materials and layers under various flooding scenarios. A schematic of the pavement structures and the points in each layer selected for analysis are presented in Fig. 2. The points in the top, middle, and bottom of the base and subgrade layer were used in the evaluation of flood patterns and lateral analysis locations. The data at 0.1 m depth intervals were used in the analysis.

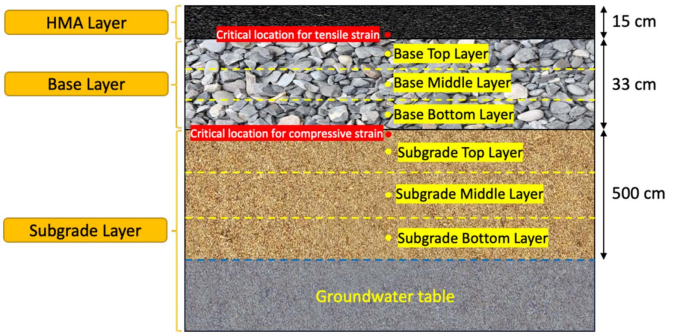

Fig. 2. A schematic of the pavement structure.

Step 2: Flood Simulation

For a simulation of a flooded pavement, FEM-based software, GEOSLOPE SEEP/W was used (GEO-SLOPE 2015). In this software, different structures were defined based on their geometry and hydraulic properties. A schematic of the structure modeled in the software along with the data output locations are shown in Fig. 3. Table 2 summarizes the hydraulic property inputs into SEEP/W. For the asphalt concrete and base layers, the hydraulic conductivity and volumetric water content (VWC) are estimated by SEEP/W

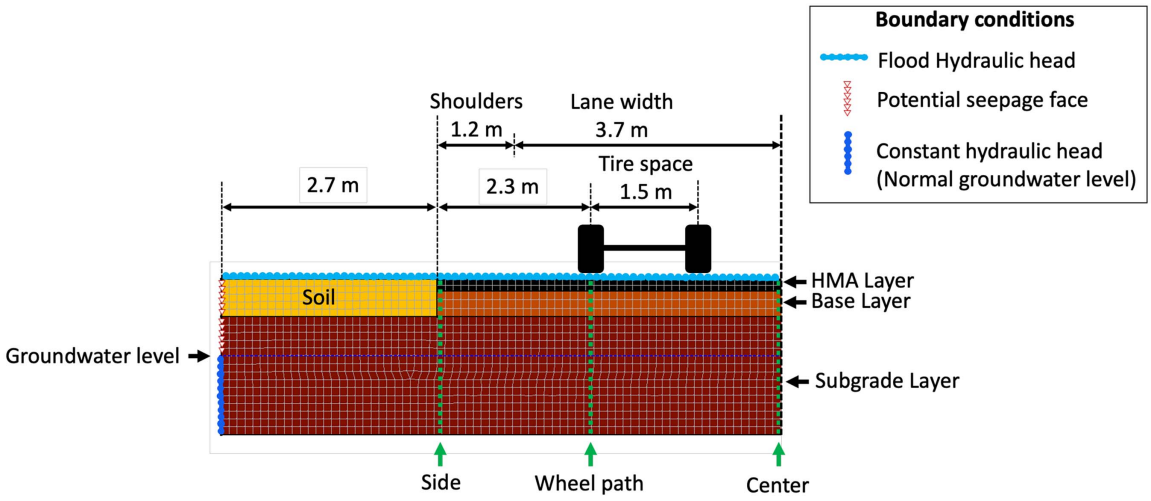

Fig. 3. A schematic of the modeled pavement structure.

according to the porosity (i.e., saturated water content) and saturated conductivity of the materials. For the subgrade (sand and clay) and organic soil, the van Genuchten models are used with material-specific parameters. The residual VWC represents the VWC of soil where a further increase in negative pore-water pressure does not produce significant changes in water content.

A flood was considered as a boundary condition in the simulation with various inundation and recession times. The inundation time begins when the flood water first overtops the pavement surface and ends when it recedes from the pavement surface. Total flood durations of 1, 2, 6, 12, and 24 h were considered in order to develop the initial framework based on short-term to long-term flooding scenarios. For flood durations of 1, 2, and 6 h, three flood heads of 0.1, 0.2, and 0.3 m on top of the surface of the pavement were considered. Initial evaluations, which are discussed in more detail in the Results and Discussion Section, showed that changing the flood head does not have as significant of an impact as the total duration. Thus, for other flood durations including 12 and 24 h, only one flood head of 0.3 m was considered, but different inundation/recession patterns were used in the analysis. These 13 different flooding scenarios are shown in Figs. 4(a and b). In order to further develop the framework based on long-term flooding scenarios, real flooding data were evaluated. The 14th flooding scenario was developed based on real groundwater depth data obtained from the United States Geological Survey (USGS) database for previous flooding events in North Carolina and New York. Different datasets were evaluated, and a pattern was detected where the groundwater reaches the surface very quickly, in a matter of days, and then takes approximately one month to return to its original level. Based on these observations, a pattern that follows the duration of the example shown for Smith Vineyard Road (47 days) and the flood head (0.55 m) of the example shown for Sunset Harbor Road was developed for real flood analysis and is shown in Fig. 5 (USGS National Water Information System 2020). This is one pattern developed based on the datasets evaluated by the authors, other patterns can be investigated using the developed framework in future work.

To demonstrate the moisture levels in the pavement during and after flooding, Fig. 6 shows the FEM mesh, flood levels, and VWC in the pavement with sand subgrade under the 0.3 m, 6 h flood as an example. The water flow direction is represented by the arrows, and the flow velocity is shown by the relative length of the arrows. Fig. 6(a) shows that the asphalt concrete is almost impermeable as the hydraulic conductivity is comparatively low (see Table 2). The floodwater enters the pavement primarily through the organic

Table 2. Hydraulic properties

Material	α (kPa)	n	Residual water content, θ_r	Saturated water content, θ_s	Saturated conductivity, k_s (m/s)
Asphalt concrete	—	—	—	0.03	9.83×10^{-10}
Gravel	—	—	—	0.20	3.00×10^{-3}
Sand	0.68	2.68	0.045	0.43	8.25×10^{-5}
Clay	12.26	1.09	0.068	0.38	5.55×10^{-9}

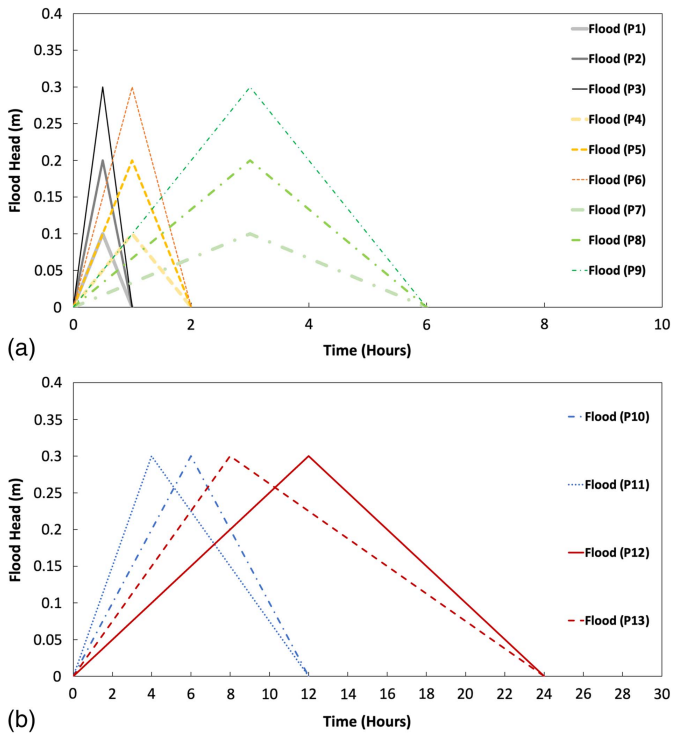

Fig. 4. Thirteen flood scenarios: (a) scenarios P1–P9; and (b) scenarios P10–P13.

J. Transp. Eng., Part B: Pavements, 2022, 148(2): 04022011

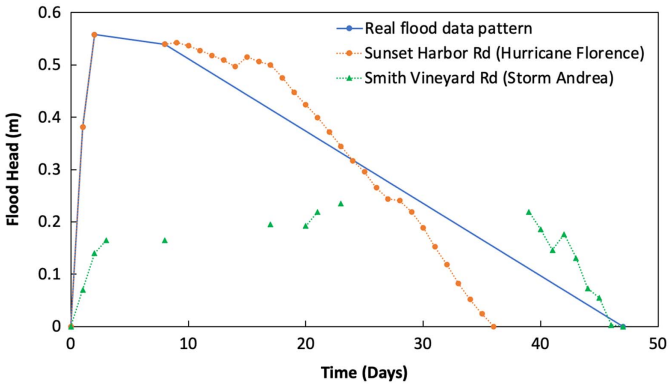

Fig. 5. Real flood data pattern as the fourteenth flood scenario.

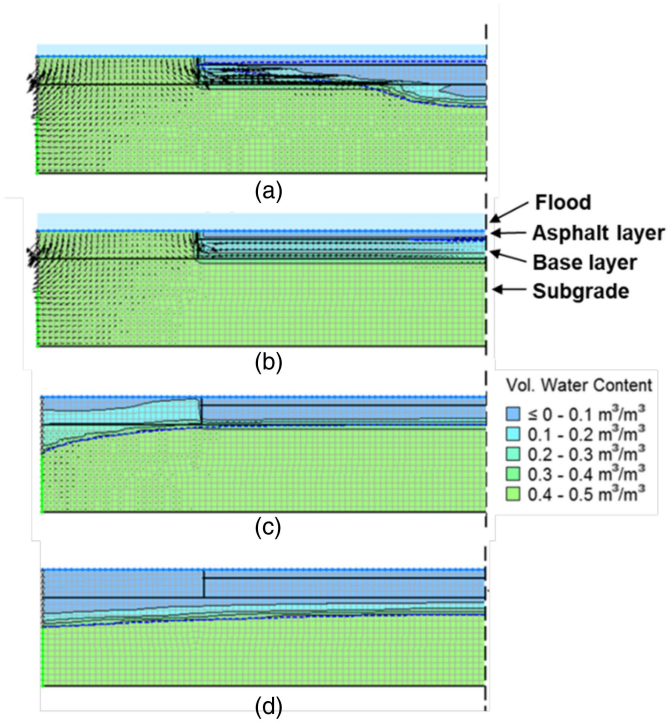

Fig. 6. Example: FEM computed volumetric (Vol.) water content for flood (0.3 m, 6 h) on pavement with sand subgrade after (a) 2 h; (b) 3 h; (c) 12 h; and (d) 1.5 days.

backfill soils and enters the base layer. The water flow velocity into the gravel base is greater than that into the subgrade (see the length of the arrows). Figs. 6(a and b) indicate that the base layer serves as a "reverse" drainage layer and allows floodwater to enter the pavement. Fig. 6(b) is when the flood depth (0.3 m) is at a maximum (3 h) and the base layer is nearly fully saturated. After 12 h, the water in the base layer infiltrates into the organic soils and subgrade. The base layer moisture has completely recovered from the flooding [Fig. 6(c)]. After 1.5 days [Fig. 6(d)], the whole pavement structure is almost recovered from the flooding, but the groundwater level is still gradually decreasing.

Step 3: Extract Water Content and Determine Resilient Modulus (M_r)

The water content from different analysis time intervals and different depths were extracted from three lateral locations including under wheel path, the center of the roadway, and the side of the roadway. Water content was converted to the degree of saturation (DOS) and then DOS was converted to the resilient modulus (M_r) using Eqs. (1) and (2). The model parameters used in Eq. (2) (Witczak equation) are presented in Table 3 (Witczak et al. 2000)

Table 3. Witczak model parameters

Parameter	Course (sand and gravel)	Fine (clay)
a	−0.3123	−0.5934
b	0.3	0.4
k	6.8157	6.1324

$$DOS = \frac{V_w}{V_v} = \frac{\theta}{\varphi} = \frac{\theta}{\theta_s} \tag{1}$$

where V_w, V_v, φ, and θ_s = volume of water, volume of void, porosity, and saturated water content (see Table 2), respectively

$$\log \frac{M_R}{M_{R,opt}} = a + \frac{b-a}{1+\exp[ln\frac{-b}{a} + k(S - S_{opt})]} \tag{2}$$

where M_R, $M_{R,opt}$, S_{opt}, and S = stiffness, stiffness at optimum water content (original stiffness was used), DOS at the optimal water content, and DOS, respectively. a, b, k are model parameters (see Table 3).

Step 4: Mechanical Response

Changes in resilient modulus result in different responses of the pavement structure under loading. Kenlayer (linear elastic analysis) was used to determine critical strains: tensile strain at the bottom of the AC layer and compressive strain on top of the subgrade layer (Fig. 2). The tensile strain and compressive strain are related to fatigue and rutting distress, respectively. In this analysis, the equivalent single axle load (ESAL, equivalent to 80 kN) was applied with a contact radius of 150 mm. WinJULEA was also used for several cases to verify the results (Huang 2004). This analysis is conducted for the multiple time intervals corresponding to the time intervals defined in the FEM analysis to determine the changes in pavement response over time.

Step 5: Damage Analysis

The calculated strains can be converted to the traffic bearing capacity (number of load repetitions to failure) at a particular time period using transfer functions. Different fatigue and rutting models have been developed by different organizations to relate the critical strains to the number of load repetitions to pavement failure. The most common forms of the fatigue and rutting failure models are presented in Eqs. (3) and (4)

$$N_f = f_1(\varepsilon_t)^{-f_2} \tag{3}$$

$$N_r = f_3(\varepsilon_v)^{-f_4} \tag{4}$$

where N_f = allowable number of load repetitions to prevent fatigue cracking from reaching a certain limit (e.g., 10–20% of the pavement surface area); N_r = allowable number of load repetitions to prevent rutting from reaching a certain limit (e.g., 0.5 in.); ε_t = tensile strain on the bottom of the asphalt layer; ε_v = compressive vertical strain on the surface of subgrade; and f_1, f_2, f_3, f_4 = regression coefficients. Depending on material type, environment, traffic conditions, and the failure limits specified by the agency, the values of the regression

Table 4. Fatigue and rutting transfer functions

Model type	Organization	f_1	f_2	f_3	f_4
Fatigue model	Illinois Department of Transportation (ILDOT)	5.00×10^{-6}	3.00	N/A	N/A
	Belgian Road Research Center (BRRC)	4.92×10^{-14}	4.76	N/A	N/A
	Transport and Road Research Laboratory (TRRL)	1.66×10^{-10}	4.32	N/A	N/A
Rutting model	Asphalt Institute (AI)	N/A	N/A	1.36×10^{-9}	4.48
	Belgian Road Research Center	N/A	N/A	3.05×10^{-9}	4.35
	Transport and Road Research Laboratory	N/A	N/A	1.13×10^{-6}	3.75
	Shell Research (SR)	N/A	N/A	6.15×10^{-7}	4.00
	US Army Corps of Engineers (USACE)	N/A	N/A	1.81×10^{-15}	6.53

Source: Data from Behiry (2012).

coefficients vary (Behiry 2012). The regression coefficients for different transfer functions are presented in Table 4.

In this study, these were used to determine how the choice of the transfer function can change the damage results and the variation of the results. The bearing capacity can be calculated for multiple time intervals, and based on Miner's rule [Eq. (5)], the cumulative damage can be calculated. In this analysis, traffic levels of 2 million ESALs and 12 million ESALs for structures with clay and sand were considered, respectively. The traffic levels were determined corresponding to the properties of structures in order to better capture more realistic pavement responses. The damage due to flooding was quantified by subtracting the damage in a normal situation (without flood) from the damage under flood conditions [Eq. (6)]

$$Damage = \sum_{i=1}^{n} \frac{n_i}{Nf_i} \tag{5}$$

where $Damage$ = cumulative damage after $\sum_1^n n_i$ load repetitions; n_i = load repetitions during period i; and Nf_i = number of load applications to failure for period i

$$\Delta Damage = Damage_w - Damage_{wo} \tag{6}$$

where $\Delta Damage$, $Damage_w$, and $Damage_{wo}$ = cumulative damage incurred by flooding, estimated cumulative damage with flooding, and estimated cumulative damage without flooding, respectively. The cumulative damage is calculated for the duration at which the traffic is allowed to pass the roadway, i.e., starting immediately after the flood water recedes to the end of the analysis period. This calculation was formed in this way in order to determine the impact of opening a flooded roadway to traffic immediately after the flood water recedes, as happens most often in practice.

Step 6: Serviceability and Cost Analysis

Since the AASHTO equation [Eq. (7)] (Huang 2004) relates the resilient modulus to the serviceability of the pavement, changes in resilient modulus were translated into changes in the long-term serviceability [represented by present serviceability index (PSI)] of the pavement due to flooding. A flood might happen in a short amount of time, but it can have a long-lasting effect on the pavement structure. To generate the PSI–time curve, the SN for each structure and traffic for monthly intervals were calculated. M_r was considered to be a constant value of 10000 psi and 4000 psi for structure with sand and clay, respectively, for the analysis except for the intervals that the M_r dropped and recovered due to flood impacts. The initial PSI value of 4.3 was considered, and incremental terminal PSI (p_t) at each interval was calculated. First, the derivative of the AASHTO equation is calculated in Eqs. (7*a*)–(7*e*) and then the incremental p_t is calculated in Eq. (7*f*). The log time

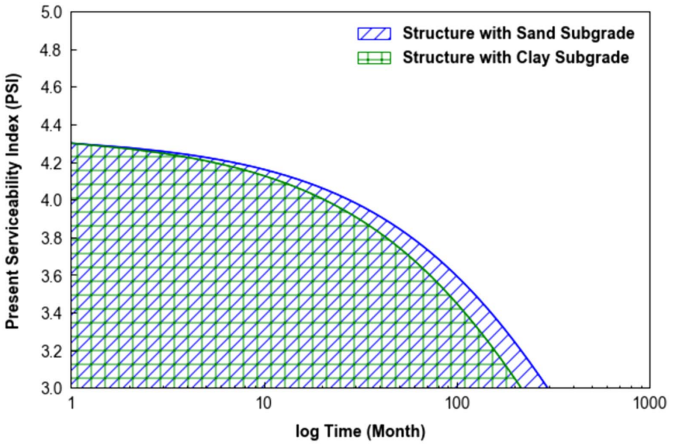

Fig. 7. Comparison of the benefit of using different structures.

versus PSI at each month was plotted. Change in serviceability was converted into a simplified cost-benefit analysis by assuming the cost of reconstruction based on the unit costs provided by PaLATE 2.0 and the benefit of using different structures. For the reconstruction cost, the total volume of the pavement structure including wearing course, base, embankment, and shoulder volume per mile (sand or clay) were calculated. They were multiplied by the suggested density value in PaLATE 2.0 and by the suggested unit costs to estimate simplified reconstruction costs. The benefit of using each structure can be represented by the area under the PSI–time curve. For instance, Fig. 7 shows that the serviceability of the structure with clay reaches the value of 3 earlier and therefore the area under the curve is smaller and can be translated into having less benefit compared to the structure with the sand subgrade

$$G_t = \log\left(\frac{p_i - p_t}{p_i - p_f}\right) = \beta_x(\log W_{tx} - \log \rho_x) \tag{7a}$$

$$p_t = p_i - (p_i - p_f)\left(\frac{ESALs_{Cumulative}}{\rho_{18}}\right)^{\beta_{18}} \tag{7b}$$

$$\rho_{18} = 10^{(9.36\log(SN+1)-0.2+2.32\log(Mr)-8.07)} \tag{7c}$$

$$\beta_{18} = 0.4 + \frac{1094}{(SN+1)^{5.19}} \tag{7d}$$

$$\frac{dp_t}{dESALs} = -(p_i - p_f)\frac{1}{(\rho_{18})^{\beta_{18}}}(\beta_{18})(ESALs_{Cumulative})^{\beta_{18}-1} \tag{7e}$$

$$p_t = p_i + \left(\frac{dp_t}{dESALs} \times \Delta ESALs\right) \quad (7f)$$

where SN = structural number; w_{18} or ESALs is the number of standard single axle load applications; M_r = resilient modulus; p_i = initial serviceability index; p_t = terminal serviceability index; and p_f = failure serviceability index.

Results and Discussion

Based on the methodology described above, the analysis was conducted and the impact of flood depth, flood time, flood pattern, real flood data, transfer function, pavement material, analysis location, pavement serviceability, and cost on various pavement structures were evaluated. The results are summarized and discussed in the following sections.

Analysis Location

Three locations were considered for the LEA including under the wheel path, in the center of the roadway, and on the side of the roadway shown in Fig. 3. The resilient moduli for different depths (defined in Fig. 2) at these three lateral locations vary, as shown for one example in Fig. 8. Specifically, the resilient modulus at the side of the roadway drops and recovers faster than other locations, and the drop and recovery of modulus are quicker for under the wheelpath compared to the center. Typically, the most critical location is under the wheelpath, but in reality, damage can potentially occur away from the loading location due to the load distribution with depth or at other locations due to traffic wander. In this study, loading was only considered in the wheel path; the side and center locations are outside the zone of impact from the wheel load and are not analyzed further. Future work should include the impact of traffic wander or loading at different lateral locations.

Flood Depth

The impact of flood depth is investigated in this section and compared with the impact of flood inundation time. Three flood depths of 0.1, 0.2, and 0.3 m were considered in nine flood scenarios (P1–P9), as shown in Fig. 4(a). The water content from different analysis time intervals and different depths were extracted from under the wheel path. Water content was converted to the DOS using Eq. (1). The calculated DOS is shown in Fig. 9. There are nine images for each subgrade type, corresponding to the different flood scenarios. The horizontal axis shows the time from the beginning of the flooding. There are 40 vertical columns in each image, and each column represents the DOS under the wheel path at different time periods (from the top to the bottom: asphalt concrete layer, the base layer, and the subgrade layer). In general, Fig. 9 shows that the influence of the inundation time is greater than the maximum flood depth on the saturation and recovery behavior, as the saturation patterns are more affected by inundation time than the maximum flood depth. This suggests that inundation time is a more important characteristic of flooding, compared to flood depth, to quantify the impact of flooding on pavements. Therefore, for roadway infrastructure, an (inundation) time–depth–damage function is more suitable than just a depth-damage function.

Flood Pattern and Time

In FEM simulations, two flood model patterns were considered so that the effect of the relative rate of inundation can be evaluated. The results for all structures and analysis locations showed that there is a slight difference between water contents for the different inundation rates. Fig. 10 shows an example where the modulus drops quicker in the top base layer for flood pattern with the faster inundation rate, but no differences can be detected in terms of recovery time. However, the results of damage analysis (Fig. 11) show that the fatigue and rutting damage results were the same. Therefore, for the flood durations of 12 and 24 h and the pavement structures that were considered in this analysis, the damage results are not sensitive to changing the flood pattern, but rather, total inundation time is the most important.

The effect of total flooding time-induced damage is summarized in Fig. 11. In this figure, representative flood scenarios with a total duration of 6 to 24 h with different patterns and the real flood scenario are presented. As inundation duration increases, the damage increases, and this pattern is independent of the structure, transfer function, distress type, or the analysis location. This reinforces that the inundation time plays a crucial role in the time–depth–damage function. The damage induced under the real flood scenario (much longer total inundation time) showed that the amount of both rutting and fatigue damage is significantly higher, especially for rutting damage in structures with sand subgrade, compared to damage due to shorter inundation times.

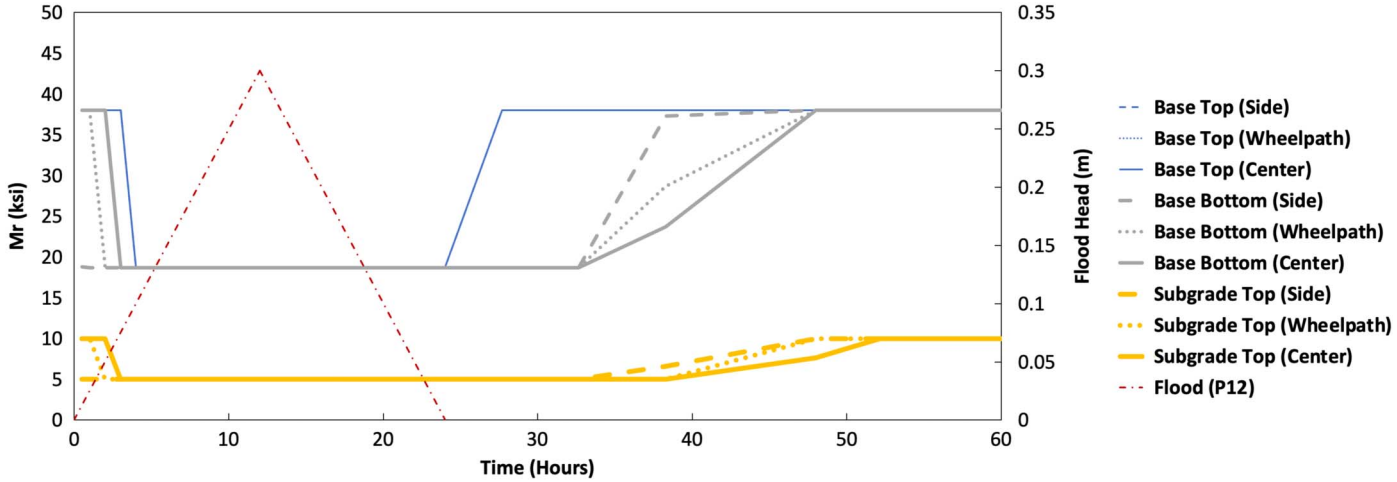

Fig. 8. Variation of resilient modulus for structure with dense-graded base and sand subgrade in different lateral and vertical locations on the road.

J. Transp. Eng., Part B: Pavements, 2022, 148(2): 04022011

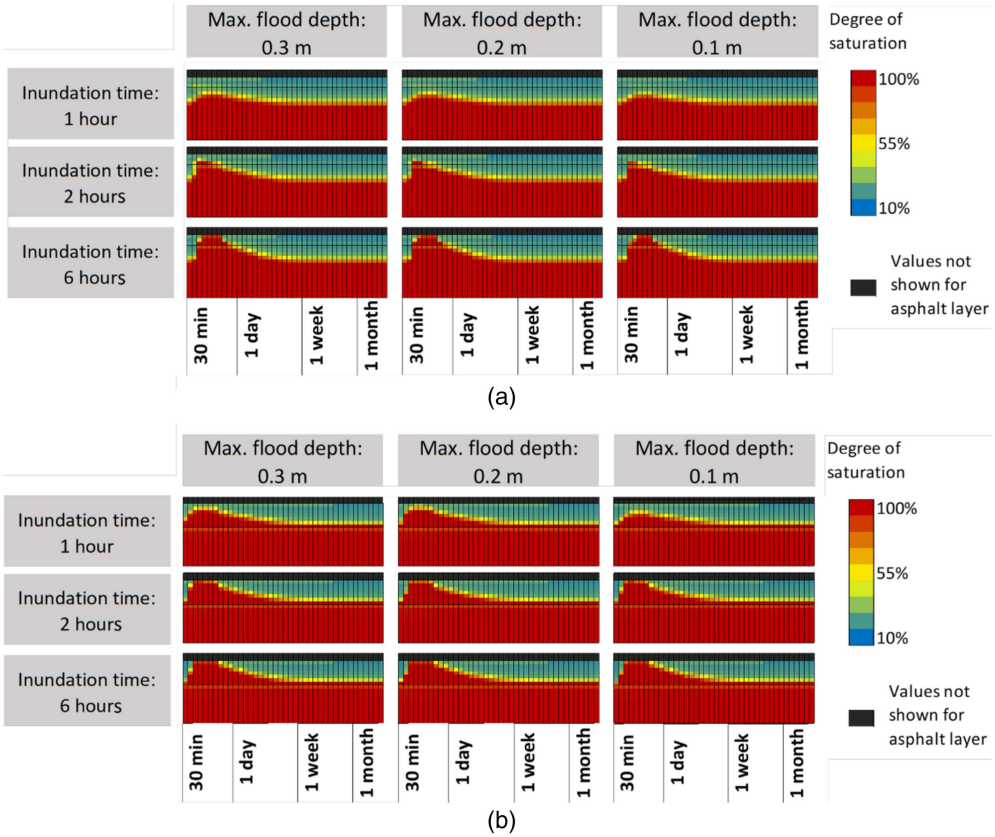

Fig. 9. Variabilities of the DOS in the pavement structure with (a) sand subgrade; and (b) clay subgrade (Max. = maximum).

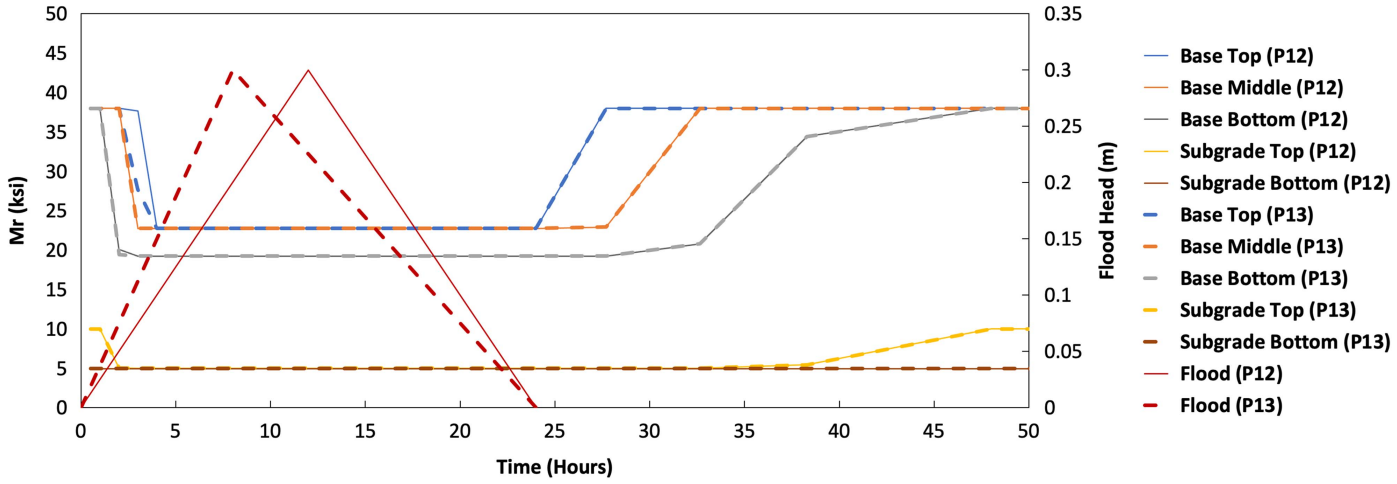

Fig. 10. Impact of changing flood pattern on resilient moduli in structure with open-graded base and sand subgrade.

Pavement Material

This section discusses the impact of the different materials within the pavement structure, drawing from the results shown in Fig. 11. The clay subgrade results in a larger percent increase in fatigue and rutting damage due to flooding than the sand subgrade. In structures with sand subgrade, open-graded gravel base material results in less additional damage than a dense-graded gravel base. The ability of the open-graded base material to more quickly drain the floodwater results in a lower amount of flood-induced damage. The opposite trend is observed for clay subgrades with the open-graded base courses showing a larger increase in damage. The low permeability of the dense-graded gravel does not allow the water to saturate the subgrade at the time of analysis and hence less damage occurs (Fig. 11). The time component related to saturation is clearly illustrated as the difference in damage increase between dense-graded and open-graded is more for the 6 h flood duration than the 24 h flood duration. This indicates that the effect of the base material is more significant for short-term floods for structures with clay subgrades. It means that during a short-term flood, the moisture content in the dense-graded base increases much slower

J. Transp. Eng., Part B: Pavements, 2022, 148(2): 04022011

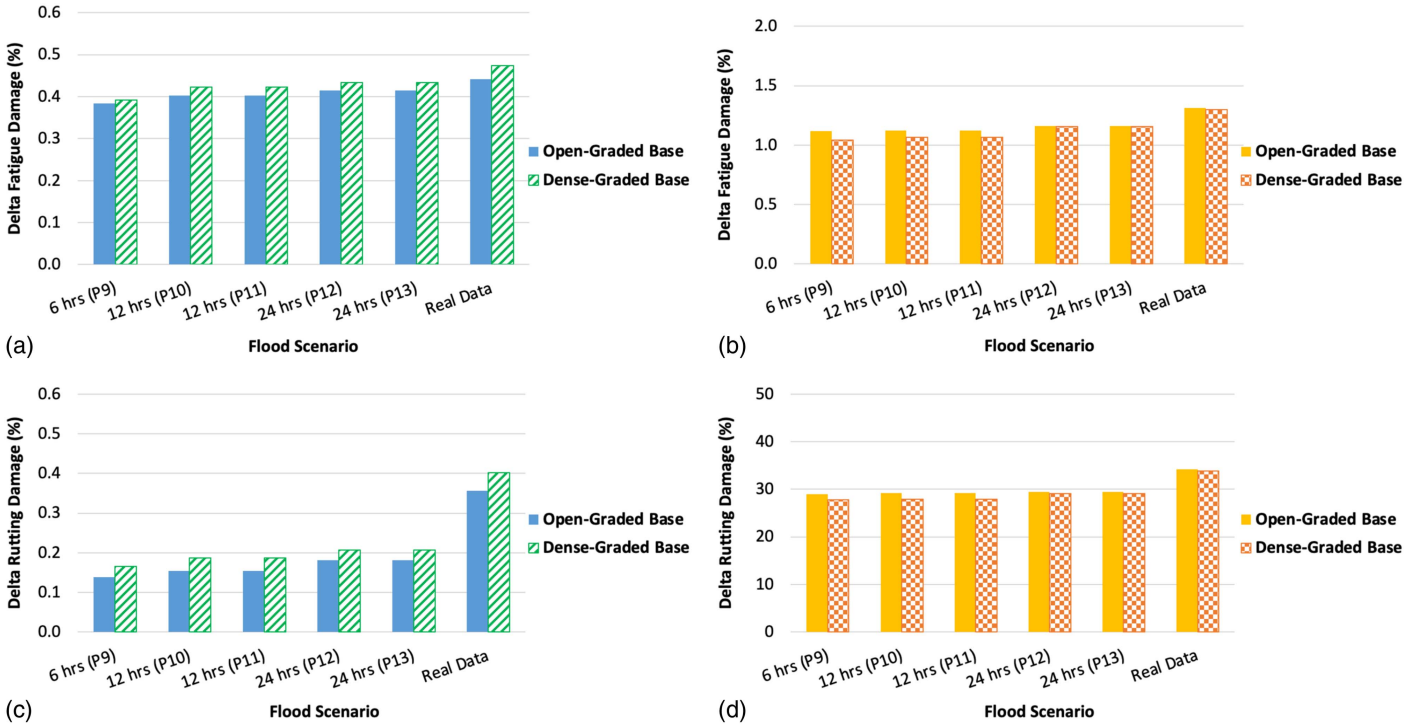

Fig. 11. Impact of variation in flood scenario on damage: (a) percent increase in fatigue damage on structures with sand subgrade; (b) percent increase in fatigue damage on structures with clay subgrade; (c) percent increase in rutting damage on structures with sand subgrade; and (d) percent increase in rutting damage on structures with clay subgrade.

than the open-graded base which results in more damage to the structure with the open-graded base. As the duration of flood increases, the difference between these structures (dense-graded and open-graded) decreases because the moisture has time to migrate into the dense-graded base. Therefore, using an open-graded base with a clay subgrade does not necessarily reduce damage as compared to using a dense-graded base. The same trend with respect to the combination of base and subgrade material types was observed with the real flood pattern.

Transfer Functions

Critical strains (tensile strain on the bottom of the AC layer and vertical strain on top of the subgrade layer) were converted to the allowable number of load repetitions using different transfer functions as part of the damage analysis. To determine the variability of different transfer functions, the coefficient of variation (COV) of changes of fatigue and rutting damage was calculated for all assumed and real flood data for different structures. The standard deviation and average of the change in damage due to flood scenarios were calculated, and the standard deviation divided by the average multiplied by 100 equals the COV. As shown in Fig. 12, the ranges of COV for fatigue and rutting damages vary significantly by changing the transfer functions. The variation in delta fatigue damage is the largest for the structure with dense-graded base and clay subgrade, but the least variation is seen in the structure with open-graded base and sand subgrade. Also, in terms of delta rutting damage, the highest variation is seen in structures with open-graded base and sand subgrade, but the structure with open-graded base and clay subgrade shows the least variation. This indicated that the choice of the transfer function can have a significant impact on the resulting change in damage depending on the type and combination of pavement materials. Therefore, in order to have some level of confidence in defining the extent of damage due to flooding, it is suggested that the transfer function that best reflects the local materials and experience be used. In the current study, the focus of the discussion and interpretation is on the results that were calculated by commonly used transfer functions [Illinois Department of Transportation (ILDOT) fatigue model and Asphalt Institute (AI) rutting model].

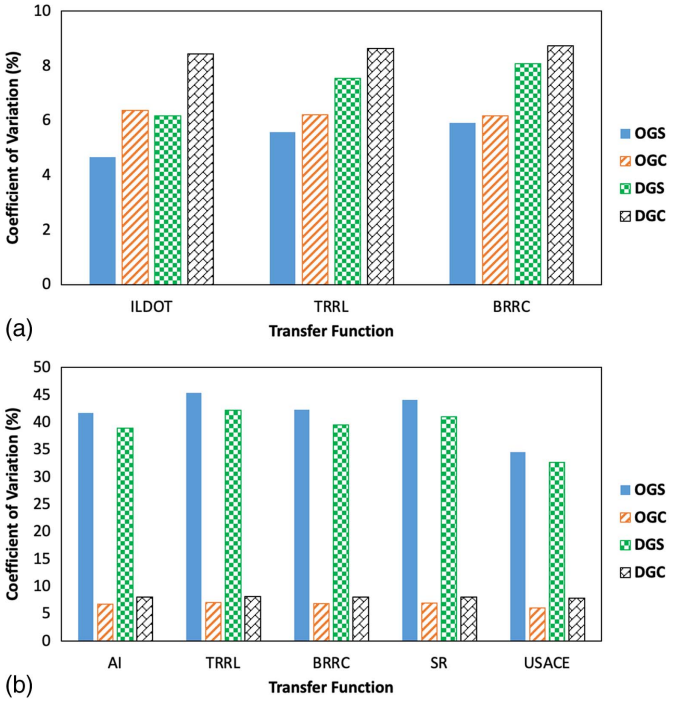

Fig. 12. Variation due to transfer functions in (a) delta fatigue damage; and (b) delta rutting damage.

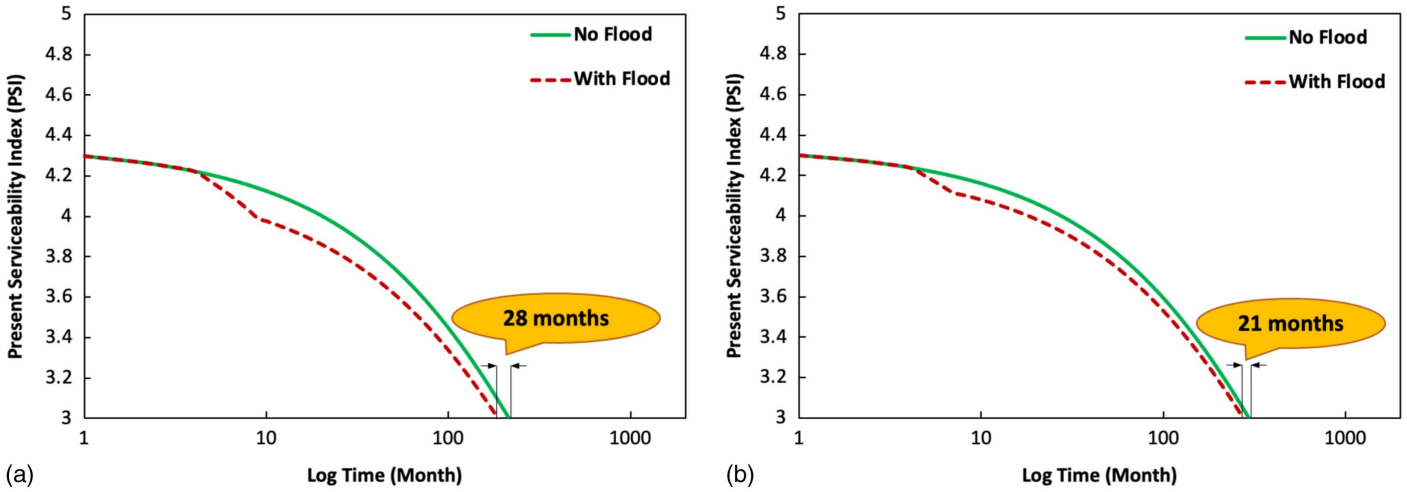

Fig. 13. Changes of pavement serviceability due to flood in one life cycle for structure with (a) clay subgrade; and (b) sand subgrade.

Pavement Serviceability

The impact of flooding on the pavement serviceability, in terms of PSI, was analyzed using the data from the real flood pattern. The analysis showed that the differences in the PSI–time curves with the two different base materials were minimal, so only the results for the open-graded base are presented in Fig. 13. For both subgrade types, the flood event causes a loss in life that will require that rehabilitation or maintenance be performed earlier than projected or planned. The life loss for structure with sand subgrade was 21 months which is the equivalent of 7.1 percent of the analysis lifetime—the time between initial and terminal serviceability of the pavement i.e., the time between PSI of 4.3 and 3. The difference in this timing is greater for the clay subgrade, which is 28 months or 13 percent of the analysis lifetime. This indicates that pavements with clay subgrades may require more frequent maintenance if the road is opened to traffic immediately after the flood water recedes.

Cost Analysis

Changes in serviceability were converted into a simplified cost-benefit analysis by calculating the cost of reconstruction based on the unit costs provided by PaLATE 2.0 and considering the area under the PSI–time as the benefit. The process of calculating the benefit-cost ratio is summarized in Table 5. The process of calculation is only presented here as a sample approach to determining the relative difference of benefit-cost ratio using the specific pavement structures and materials examined in this study. The results show that the difference between the benefit-cost ratio due to flooding for structures with clay subgrade is more considerable than structures with sand subgrade. The benefit-cost ratio for the clay subgrade drops by almost 15% after one inundation period, whereas the benefit-cost ratio for the sand subgrade only drops by about 8%. This analysis indicates that opening the roadway to traffic immediately after floodwaters recede will cost more to reconstruct, especially for structures with clay subgrades, than waiting for the pavement to recover. This type of information should be included in the decision-making process and also accounted for in the budget allocations (Qiao et al. 2017).

Uncertainties of the Analysis

The main objective of this study is to introduce the concept and framework to develop time–depth–damage functions. The development of these functions is still in the preliminary stages and therefore, many assumptions were made in the study. Assumptions in the FEM model consist of assumed flooding scenarios, aggregate/subgrade soil moduli, and traffic loading. These assumptions shall be addressed by establishing validation measures in the laboratory or with respect to actual field sites. Damage cost assumptions refer to the assumptions on the costs of the damaged road. Such costs shall be obtained from the postflooding survey of the damaged road and the actual cost of the road construction. Other assumptions are out of the quantification capability of the established model, e.g., damage quantification of the washout effects. Separate models (e.g., a washout damage model) should be established to account for the damage caused by conditions not addressed in this work. The aforementioned assumptions need to be refined further in future studies.

Sensitivity analysis is required to account for the possible inherent limitations of various models chosen in the analysis process, including the FEM models and empirical models (e.g., Witczak equation and damage transfer functions). Uncertainties in these models can certainly accumulate in the modeling system and can impact the results. However, the priority focus of this work is to develop the framework; prediction accuracy will be part of the efforts in future work and will be important in a final tool. To examine to what extent variations in inputs and selected models impact the results, the sensitivity of the results (e.g., predicted moisture levels)

Table 5. Benefit-cost analysis

Structure	Condition	Benefit	Discount rate	Months to PSI = 3	Initial cost	Reconstruction cost	PV cost	B/C
Clay subgrade	No flood	6,104,419	0.04	215	199,686	199,686	199,729	31
	Flood	5,233,674	0.04	187	199,686	199,686	199,816	26
Sand subgrade	No flood	50,992,500	0.04	295	198,428	198,428	198,430	257
	Flood	47,006,500	0.04	274	198,428	198,428	198,432	237

J. Transp. Eng., Part B: Pavements, 2022, 148(2): 04022011

to variations in the FEM inputs, parameters of the empirical models, and different boundary conditions need to be evaluated.

Summary and Conclusions

A framework for developing time–depth–damage functions to model postflooding road damage in flexible pavement structures due to moisture increases in unbound layers is proposed in this study. The framework is developed based on seepage modeling using the FEM, established relationships between layer stiffness and moisture content, multilayer elasticity theory, and damage transfer functions. The objective of this study is to develop a methodological framework for establishing time–depth–damage functions using the synthetic approach. The main contribution of this study is that it enables the quantification of flood-induced damage on pavements, which is a current gap in the field. Various factors that can impact flooding induced pavement damage are considered in this study; specifically, this work is designed to identify the importance of several parameters including flood duration, flood depth, flood pattern (including real flood data), the transfer function for damage calculation, pavement material, and analysis location. In addition, pavement serviceability and costs are evaluated. The long-term goal is a tool for decision makers to use in planning and management of flooding events for more resilient flexible pavements and allocation of budgets. For this purpose, four structures with the same thickness and different materials including open-graded and dense-graded gravel for base and sand and clay for subgrade were considered. These structures were evaluated under 13 flood scenarios from 1-h to 24-h flood time with different patterns and one flood scenario representative of real flood data. The water content as a function of time in the pavement layers at different depths and lateral locations was determined using FEM-based hydraulic analysis software for the different flood scenarios. The water content values were converted to resilient modulus, and LEA was conducted to translate the changes in modulus to changes in critical strains. These were then converted to damage using different transfer functions considering the road was opened to traffic immediately after the floodwater recedes. The changes in fatigue and rutting damage and pavement serviceability due to flooding for different structures and flood scenarios were evaluated. The cost-benefit analysis was done using the pavement serviceability curves and calculated construction costs using typical values. The main conclusions of this study, specific to the inputs and assumptions, are the following:

- Inundation time is a more important factor than flood depth to determine postflooding pavement damage under traffic due to loss of stiffness.
- Flood duration has a significant impact on the amount of damage. The results showed that total inundation time plays a crucial role and must be included in flooded pavement damage functions.
- Overall, structures with clay subgrade experienced more fatigue and rutting damage, earlier and more significant loss of serviceability, and considerable loss of benefit-cost ratio due to flood as compared to structures with sand subgrades.
- The performance of the combination of the materials subjected to flood is more important than the properties of the materials individually. The results indicated that the combination of sand and open-graded gravel or clay and dense-graded gravel placed as subgrade and base layer in pavement structure are more resilient.
- The performance of the combinations of materials in the subgrade and base layers is more critical in short-term floods since the difference in both fatigue and rutting damage between the combination of open-graded gravel/sand and dense-graded gravel/sand is more significant with 6 h inundation time compared to 24 h inundation time.
- For the flood durations of 12 and 24 h, the damage results were not sensitive to changing the rate of inundation, but rather total inundation time played a key role. There was a slight difference between resilient moduli with different inundation rates, but no significant differences were detected in damage results.
- The range of fatigue and rutting damage varies significantly by changing the transfer functions and choice of the transfer function can have a significant impact on the resulting change in damage depending on the type and combination of pavement materials.
- The resilient modulus from under wheel path, on the center of the roadway, and on the side of the roadway vary considerably. This indicated that the damage due to flood can vary in different lateral locations, and it needs to be further considered.

It was established in this study that in time–depth–damage functions several parameters are most influential when the pavement structure is subjected to flooding events. The most important parameters are the flood duration, the combination of the materials, critical location on the roadway (both vertical and lateral), and appropriate interpretation of damage with respect to transfer functions. These parameters should be considered by decision makers for planning and management decisions regarding reopening the road after a flood event and budget allocations. As presented in this study, opening the roadway to traffic immediately after the flood water recedes will lead to faster degradation of the pavement and increased maintenance and rehabilitation costs.

This study had certain limitations that need to be addressed in future research studies. The procedures and influential parameters explained in this study can be used to develop generalized time–depth–damage functions that cover a practical range of pavement structures and materials, various combinations of pavement materials, more realistic flood time and pattern, the potential impact of temperature, and condition of the asphalt layer. A more detailed and robust analysis can be conducted in terms of the cost due to flooding instead of the simplified analysis. Supplementary field data is necessary to validate the findings of this study.

Data Availability Statement

Some or all data, models, or codes that support the findings of this study are available from the corresponding author upon reasonable request. Such data or models are FEM models, Kenlayer models, and algorithms used in the analysis.

Acknowledgments

The authors would like to acknowledge support from the University of New Hampshire Center for Infrastructure Resilience to Climate (UCIRC) and the Sustainability Fellows Program. The authors also acknowledge support from the National Natural Science Foundation of China (No. 52008388) and the Jiangsu Innovation and Entrepreneurship Doctoral Program for Dr. Qiao's time.

References

Behiry, A. E. 2012. "Fatigue and rutting lives in flexible pavement." *Ain Shams Eng. J.* 3 (4): 367–374. https://doi.org/10.1016/j.asej.2012.04.008.

Chen, X., and Z. Zhang. 2014. "Effects of hurricanes Katrina and Rita flooding on Louisiana pavement performance." In *Pavement materials, structures, and performance*, 212–221. Reston, VA: ASCE.

Daniel, J. S., et al. 2018. *Flooded pavement assessment*. FHWA-PROJ-13-0015. Washington, DC: Federal Highway Administration.

Dawson, A. 2009. *Water in road structures*. Dordrecht, Netherlands: Springer.

Elshaer, M., and J. S. Daniel. 2018. "Impact of pavement layer properties on the structural performance of inundated flexible pavements." *Transp. Geotech.* 16 (Sep): 11–20. https://doi.org/10.1016/j.trgeo.2018.06.002.

Fladvad, M., and S. Erlingsson. Forthcoming. "Permanent deformation modelling of large-size unbound pavement materials tested in a heavy vehicle simulator under different moisture conditions." *Road Mater. Pavement Des.* https://doi.org/10.1080/14680629.2021.1883464.

Gaspard, K., M. Martinez, Z. Zhang, and Z. Wu. 2007. *Impact of Hurricane Katrina on roadways in the New Orleans area*. Technical Assistance Rep. No. 07-2TA. Baton Rouge, LA: Louisiana DOT and Development, Louisiana Transportation Research Center.

GEO-SLOPE. 2015. *Seepage modeling with SEEP/W. SEEP/W user manual*. Calgary, Canada: GEO-SLOPE International Ltd.

Huang, Y. H. 2004. *Pavement analysis and design*. 2nd ed. Saddle River, NJ: Pearson.

Khan, M. U., M. Mesbah, L. Ferreira, and D. J. Williams. 2017. "Estimating pavement's flood resilience." *ASCE Transp. Eng. J.: Part B: Pavements* 143 (3): 04017009. https://doi.org/10.1061/JPEODX.0000007.

Mallick, R., M. Tao, J. Daniel, J. M. Jacobs, and A. Veeraragavan. 2017. "A combined model framework for asphalt pavements condition determination after flooding [poster presentation]." In *Proc., Transportation Research Board 96th Annual Meeting*, 64–72. Washington, DC: Transportation Research Board.

Nadal, N. C., R. E. Zapata, I. Pagán, R. López, and J. Agudelo. 2010. "Building damage due to Riverine and coastal floods." *J. Water Resour. Plann. Manage.* 136 (3): 327–336. https://doi.org/10.1061/(ASCE)WR.1943-5452.0000036.

Pistrika, A., G. Tsakiris, and I. Nalbantis. 2014. "Flood depth-damage functions for built environment." *Environ. Process.* 1 (4): 553–572. https://doi.org/10.1007/s40710-014-0038-2.

Pistrika, A. K., and S. N. Jonkman. 2010. "Damage to residential buildings due to flooding of New Orleans after Hurricane Katrina." *Nat. Hazards* 54 (2): 413–434. https://doi.org/10.1007/s11069-009-9476-y.

Qiao, Y., R. A. Medina, L. M. McCarthy, R. B. Mallick, and J. S. Daniel. 2017. "Decision tree for postflooding roadway operations." *Transp. Res. Rec.* 2604 (1): 120–130. https://doi.org/10.3141/2604-15.

Romanoschi, S. 2019. *The impact of Hurricane Harvey on pavement structures in the South East Texas and South West Louisiana*. Final Rep. Project No. 18PUTA02. Arlington, TX: Univ. of Texas at Arlington.

Salour, F., and S. Erlingsson. 2013. "Moisture-sensitive and stress-dependent behavior of unbound pavement materials from in situ falling weight deflectometer tests." *Transp. Res. Rec.* 2335 (1): 121–129. https://doi.org/10.3141/2335-13.

Scawthorn, C., et al. 2006. "HAZUS-MH flood loss estimation methodology. II. Damage and loss assessment." *Nat. Hazard. Rev.* 7 (2): 72–81. https://doi.org/10.1061/(ASCE)1527-6988(2006)7:2(72).

Sultana, M., G. Chai, T. Martin, and S. Chowdhury. 2016. "Modeling the postflood short-term behavior of flexible pavements." *J. Transp. Eng.* 142 (10): 04016042. https://doi.org/10.1061/(ASCE)TE.1943-5436.0000873.

Texas DOT. 2019. *Asset management, extreme weather and proxy indicators pilot*. Austin, TX: Federal Highway Administration.

USGS National Water Information System. 2020. Accessed August 30, 2020. https://waterdata.usgs.gov/nc/nwis/current/?type=gw.

Vennapusa, P. K. R., D. J. White, and D. K. Miller. 2013. "*Western Iowa Missouri River flooding—Geo-infrastructure damage assessment, repair and mitigation strategies*. Washington, DC: Iowa Highway Research Board and Federal Highway Administration.

Witczak, M. W., D. Andrei, and W. N. Houston. 2000. *Guide for mechanistic-empirical design of new and rehabilitated pavement structures appendix DD-1: Resilient modulus as function of soil moisture-summary of predictive models*. NCHRP Project 1-37A. Washington, DC: Transportation Research Board.

Zhang, Z., Z. Wu, M. Martinez, and K. Gaspard. 2008. "Pavement structures damage caused by Hurricane Katrina flooding." *J. Geotech. Geoenviron. Eng.* 134 (5): 633–643. https://doi.org/10.1061/(ASCE)1090-0241(2008)134:5(633).